Characterization of the Reaction Products of Laser-Ablated Late Lanthanide Metal Atoms with Dinitrogen. Matrix IR Spectra of LnN, $(LnN)_2$, and $Ln(NN)_x$ Molecules

Stephen P. Willson and Lester Andrews*

Chemistry Department, University of Virginia, Charlottesville, Virginia 22901

Received: October 26, 1998; In Final Form: January 8, 1999

This paper comprises the final section of a two-part study of the small nitride molecules and simple dinitrogen complexes of the lanthanide metals, except promethium. Simple nitrides of the general formulas LnN and $(LnN)_2$ have been identified for Ln = Tb, Dy, Ho, Er, Tm, Yb, and Lu. Further elucidation of the $Ln(N_2)$ and $Ln(NN)_2$ complexes is presented. The evidence supports the anticipated conclusion that the later lanthanide metals are less prone to dinitrogen complexation and that the nitrides of the later lanthanide metals require fewer dinitrogen units to achieve saturation.

Introduction

This study of reactions of late lanthanide metal atoms with dinitrogen is being undertaken to increase the chemical knowledge of simple reactions of lanthanide metal atoms with gaseous dinitrogen, about which relatively little is known, although these metals and their compounds are of burgeoning importance in modern technologies.[1−5] The matrix-isolation method is employed to provide a snapshot of the reacting systems, allowing analysis of precursors, intermediates, and products involved. Further annealing and broadband ultraviolet photolysis of samples collected provides information about the continuance of the observed reactions from the original frozen state. There is significant evidence in the literature demonstrating that infrared vibrational frequencies obtained for molecules trapped in a solid argon cage are generally good approximations of the gas-phase frequencies of the free molecules; specific to this case is the strong correlation demonstrated between the transition metal mononitride frequencies observed both in inert matrices and in the gas phase.[6−12] Although the products reported here have not been identified in the gas phase, precedent set by previous spectroscopic assignments suggests that argon matrix frequencies are about 10 cm^{-1} lower and are, therefore, reasonable predictors of the gaseous values.

As with the early lanthanide metal atoms, part 1 of this series,[13] the late lanthanide metal atoms also show the proclivity toward complexing and reducing dinitrogen, forming nitride rings containing two N atoms and two metal atoms without residual N−N bonding, i.e., $Ln(\mu\text{-}N)_2Ln$. This scission of the dinitrogen bond by two naked metal atoms has not been achieved by other methods, although many inorganic complexes containing a similar ring structure have been identified in the past decade.[14−16]

Experimental Section

Lanthanide atoms supplied by laser vaporization of a metal target were reacted with molecular nitrogen in both argon and nitrogen matrices using techniques described in previous publications.[17−20] Experiments carried out in solid nitrogen films required sample deposition periods of 15−25 min; in argon, with N_2 concentrations ranging from 2 to 4%, about 1 h was required. Both types of experiments worked well with deposition rates of about 5 mmol/h onto a CsI window held at 6−7 or 10−11 K. Infrared spectra were recorded at 0.5 cm^{-1} resolution with a Nicolet 750 or 550 spectrometer after deposition and after each annealing or photolysis. The metal targets, Tb, Dy, Ho, Er, Tm, Yb, and Lu (all Johnson−Matthey 99.9%), were ablated with the 1064-nm fundamental of a YAG laser using 35−50 mJ pulses. For some experiments, isotopically scrambled N_2 was created by flowing the gas mixture through a microwave discharge (20 W) in a 6 mm o.d. quartz tube. Following deposition, argon matrices were annealed to 28K, nitrogen matrices to 25 K, and then subjected to UV photolysis using a 175-W mercury street lamp (Philips H39KB) without the globe (240−580 nm). An annealing cycle consists of raising the matrix temperature to the specified value and then lowering back to the deposition temperature of 6−7 or 10−11 K. Two or three additional annealings were then done, not exceeding 45 K for argon matrices or 35 K for nitrogen films, and additional spectra were recorded.

Results

The absorptions observed in all seven of these metal nitride systems can be divided into three general regions of the infrared spectrum. There are several products that absorb in the traditional metal nitride stretching region between 450 and 1000 cm^{-1}, three of which show nitrogen 14/15 ratios appropriate for Ln−N stretching modes. Absorptions that occur from 1200 to 2400 cm^{-1} are in the expected region for N_2 complexes and show the appropriate 14/15 ratios for N−N stretching frequencies. In general, these bands increase upon annealing, but are not significantly affected by photolysis. In addition, absorptions observed in nitrogen films near 3400 cm^{-1} are in the region expected for overtones of dinitrogen complexes. Observed product peaks for each of the subject metals are fully delineated in Tables 1−7 and include N_3 radical and anion in pure dinitrogen,[20,21] and weak metal oxide bands identified from separate oxide studies.[22−24] Figures 1−5 show examples of important regions in the spectra. Results of successive annealing cycles are included in the tables; photolysis data is also included when it provides useful information. Where matrix sites are present, only the primary peak is considered in the text.

Discussion

As with the previous paper, the discussion is divided into two main portions, metal nitrides and metal dinitrogen com-

10.1021/jp984181r CCC: $18.00
Published on Web 02/24/1999

TABLE 1: Product Absorptions (cm^{-1}) Observed for Laser-Ablated Tb Atoms in Solid Matrices at 10 K

$^{14}N_2$	$^{15}N_2$	$^{14}N_2 + {}^{15}N_2$	$^{14}N_2 + {}^{14,15}N_2 + {}^{15}N_2$	$R(14/15)$[b]	anneal.[c]	ident.
			Argon[a]			
2309	2232	2309, 2232	2310, 2272, 2233	1.0345	a++0	$(NN)_x(TbN)_2$
2093.4	2024.2	2092, −		1.0342	b++	$(NN)_xTbO_2$
2034	1967	2030, 1963	2028, 1996, 1960	1.0341	b++(−)	$Tb(NN)_x$
1995.0	1929.4			1.0340	b++	$Tb(NN)_x$
1946.1	1882.0	−, 1882.0		1.0341	b++(−)	$Tb(NN)_x$
1920.5	1857.1			1.0341	a+++	$Tb(NN)_x$
1870.3	1808.3	1870.2, −		1.0343	b+−	$Tb(N_2)$
1859.5	1798.0	1859.5, 1798.0	1859.5, 1829.0, 1797.9	1.0342	b++	$Tb(N_2)$
1852.6	1791.3	1852.7, 1791.3		1.0342	a++−	$Tb(N_2)$
1846.1	1784.9	1846.2, 1785.0	1846.3, 1815.9, 1785.1	1.0343	a+++	$Tb(N_2)$
1834.0	1773.9	1833.8, 1774.0		1.0339	b++	$Tb(N_2)$
1800.1	1740.7			1.0341	b++	
1792.8	1733.1			1.0344	a000	
1789.4	1730.7			1.0339	b+−	
1767	1708	1766, 1708	1766, 1737, 1708	1.0345	b++	$(NN)_xTb(N_2)$
1751.0	1693.7	1750.8, 1693.6	1750.9, 1722.5, 1693.6	1.0338	b++	$(NN)_xTb(N_2)$ site
1746.2	1688.5	1746.2, 1707.4, 1688.5	1746.3, 1729.3, 1717.6, 1707.5, 1700.4, 1688.5	1.0342	a− − −	$Tb(NN)_2$
1743.8	1686.2	1743.8, 1705.7, 1686.3	1743.8, 1727.1, 1715.4, 1706.0, 1698.3, 1686.4	1.0342	a− − −	$Tb(NN)_2$ site
1649.9	1595.3			1.0342	b++	$Tb_x(NN)_y$
1595.9	1543.3			1.0341	b++	$Tb_x(NN)_y$
1589.5	1536.9			1.0342	b++	$Tb_x(NN)_y$
1583.2	1531.0			1.0341	b++	$Tb_x(NN)_y$
1567.6	1515.7			1.0342	b++	$Tb_x(NN)_y$
1557.9	1506.3		1558, 1543, 1531, 1517, 1508	1.0343	b++	$Tb_x(NN)_y$
1553.3	1502.3			1.0339	b++	$Tb_x(NN)_y$
1542.6	1491.5			1.0343	b++	$Tb_x(NN)_y$
1534.0	1483.3			1.0342	b++	$Tb_x(NN)_y$
1525.1	1473.2			1.0352	b++	$Tb_x(NN)_y$
823.9	823.9	823.8	823.9		a− − −	TbO
805.3	780.4	805.3, 780.5	805.4, 780.6	1.0319	a+0−	TbN
765.6	765.3	764.8	764.8		b++	$(NN)_xTbO$
758.6	758.6	758.5			a+0−	TbO_2 ν_1
744.2	744.4	744.3	741.2		b++	$(NN)_xTbO_2$ ν_1
718.6	718.6	718.6			a+0−	TbO_2 ν_3
702.9	702.8	702.7	702.8		b++	$(NN)_xTbO_2$ ν_3
698.8	678.0	698.7, 678.1	698.8, 688.8, 678.1	1.0307	a− − −	$(TbN)_2$
696.9	675.8	696.8, 675.8	696.8, 686.5, 675.8	1.0312	a− − −	$(TbN)_2$
691.7	670.9	691.6, 670.8	691.6, 681.5, 670.9	1.0310	a++−	$(NN)_x(TbN)_2$
682.3	661.2			1.0319	b++	$(NN)_x(TbN)_2$
675	653	671.0, 650.7	671.4, 660.8, 650.5	1.0312	b++	$(NN)_x(TbN)_2$
569.3	552.4	569.5, 552.4	569.9, 559.6, 552.8	1.0306	a− − −	$(TbN)_2$
567.8	550.5	567.7, 550.3	567.8, 558.0, 550.4	1.0314	a− − −	$(TbN)_2$
565.1	548.1	565.1, 548.0	565.0, 555.5, 547.7	1.0310	a++−	$(NN)_x(TbN)_2$
562.4	545.3	562.1, 545.2	561.5, 552.6, 545.4	1.0314	b++	$(NN)_x(TbN)_2$
555.1	537.7	554.3, 537.2	554.2, 543.6, 537.1	1.0324	b++	$(NN)_x(TbN)_2$
502.7	487.1	501.2, 486.1	501.4, 486.9	1.0320	a− − −	Tb_2N
496.2	480.3	495.3, 480.6	496.0, 481.2	1.0331	b++	$(NN)_xTb_2N$
			Dinitrogen[a]			
3538.3	3423.0	3537, 3485, 3426		1.0337	a−0−(−)	(NN)Tb(NN) ν_3
3482.2	3368.8			1.0337	a00−	(NN)Tb(NN) ν_3
3425.6	3312.3	3426, 3314		1.0342	a0+−	$(NN)_xTb(N_2)$
2327.5	2249.6	2327.7, 2249.9	2327.7, 2289.1, 2249.9	1.0346	a−0−	N_2
2300.6	2223.7	2300.9, 2224.1	2301.0, 2262.7, 2223.9	1.0346	a++−(−)	$(NN)_x(TbN)_2$
2269.7	2194.3	2269.8, 2194.5		1.0344	a++−(−)	$Tb(NN)_x$
2139.7	2069.2	2139.5, 2069.8		1.0341	a++−(−)	$Tb(NN)_x$
2028.4	1961.8	2029.6, 1962.8	2029.4, 1995.9, 1962.4	1.0340	a−0−(+)	$Tb(NN)_x$
2022.6	1954.6	2022.5, 1955.3	2022.3, 1990.2, 1954.9	1.0348	a++−(−)	$Tb(NN)_x$
1815.4	1756.1	1814.6, 1798.6, 1793.5, −	1814.9, 1804.8, 1800.9, 1795.5, 1787.7, 1777.9, 1775.2, 1772.6	1.0338	a0+−(−)	(NN)Tb(NN) ν_1
1746.8	1689.5	1746.7, 1710.1, 1705.0, 1689.6	1746.8, 1732.5, 1727.3, 1718.7, 1711.4, 1704.0, 1698.8, 1689.8	1.0339	a0+−(−)	(NN)Tb(NN) ν_3
1726.7	1669.2	1725.5, 1669.4	−, −, 1669.6	1.0344	a0+−	$(NN)_xTb(N_2)$
1593.5	1541.1	1592.4, 1564.9, 1540.2	1592, 1579, 1567, 1552, 1538	1.0340	a− − −	$Tb^+(N_2)_2^-$
1577.9	1525.8	1578.4, 1527.3	−, −, 1524	1.0342	a− − −	$Tb_x(NN)$
1217.8	1178.1	1217.8, 1178.2	1218, 1197, 1178	1.0337	c+−	$Tb_x(NN)$
1211.6	1172.4	1211.4, 1172.2	1211, 1192, 1172	1.0334	a++−	$Tb_x(NN)$ site
764.6	740.9	764.6, 741.0	764.6, 741.0	1.0320	a++−(−)	$(NN)_xTbN$
749.7		749.6			a++−	$(NN)_xTbO_2$ ν_1
748.5		748.5			a++−	$(NN)_xTbO_2$ ν_1
709.8	709.7	709.7	709.7		a++−	$(NN)_xTbO_2$ ν_3
708.7	708.6	708.6	708.6		a++−	$(NN)_xTbO_2$ ν_3
669.4	648.9	669.2, 659.8, 649.2	669.2, 659.5, 649.1	1.0316	a+− −	$(NN)_x(TbN)_2$
550.9	534.4	551.3, 541.7, 534.8	551.5, 541.3, 534.4	1.0309	a+− −	$(NN)_x(TbN)_2$
468.6	453.9			1.0324	a00−(−)	$(NN)_xTb_2N$

[a] Matrix composition. [b] Ratio (14/15) isotopic frequencies. [c] Annealing behavior: a denotes presence on deposition, +, −, or 0 indicates the direction of growth in three successive annealings, b denotes appearance on the 1st annealing and +, −, or 0 indicates changes on 2cd and 3rd annealings, c indicates appearance on photolysis, also with changes on the 2nd and 3rd annealings, (+ or −) indicates changes on photolysis.

TABLE 2: Product Absorptions (cm^{-1}) Observed for Laser-Ablated Dy Atoms In Solid Matrices at 10 K

$^{14}N_2$	$^{15}N_2$	$^{14}N_2 + {}^{15}N_2$	$^{14}N_2 + {}^{14,15}N_2 + {}^{15}N_2$	$R(14/15)^b$	anneal.[c]	ident.
			Argon[a]			
2307	2230	2304, 2230	2310, 2270, 2236	1.0345	a+++	$Dy(NN)_x$
1809.2	1749.1	1808.8, 1748.7	1808.5, 1778.8, 1748.5	1.0344	a+− −	$Dy(N_2)$
1804.8	1744.8			1.0344	a+++	$Dy(N_2)$
1799.8	1739.9	1799.5, 1740.0	1799.5, 1770.0, 1739.9	1.0344	a+++	$Dy(N_2)$
1794.8	1735.2	1794.5, 1735.5	1794.7, 1765.2, 1735.4	1.0343	b++	$Dy(N_2)$
1770.4	1711.7			1.0343	b++	$(NN)_xDy(N_2)$
1754.2	1696.8	1754.2, 1696.7		1.0338	a000	$(NN)_xDy(N_2)$
829.0	829.0	828.6	828.8		a− − −	DyO
825.3	825.3	825.1	825.3		a− − −	DyO
822.1	822.2	822.5	822.1		a− − −	DyO
810.5	785.5	810.6, 785.6	810.5, −	1.0318	a00-	DyN
701.9	681.8			1.0295	a− − −	$(DyN)_2$
693.9	693.9	693.8	693.8		a00−	oxide
683	663	679.5, 658.8		1.0302	b++	$(NN)_x(DyN)_2$
580.3	580.2	580.2	580.4		a00−	DyO_2 ν_3
574.4	574.4	574.1	574.4		a00−	DyO_2 ν_3
570.9	571.0	570.6	571.0		a00−	DyO_2 ν_3
535.5	535.4	535.4	535.6		a− − −	oxide
505.3	489.7	504.5, 489.1	505.4, 489.7	1.0319	a− − −	Dy_2N
500	484	498.2, 482.8		1.0331	b++	$(NN)_xDy_2N$
			Dinitrogen[a]			
3536	3423			1.0333	a00−	$(NN)_xDy(NN)_2$
3487	3374	3489, 3373	3486, 3428, 3372	1.0335	a00−	$(NN)_xDy(N_2)$
2299.5	2222.7	2299.8, 2222.9	2299.8, 2261.6, 2223.0	1.0346	a+++	$(NN)_x(DyN)_2$
2120.5	2050.0		2075.8	1.0344	a− − −	$Dy(NN)_x$
1759.4	1701.0	1758.5, 1701.9	1759.1, 1731.1, 1702.1	1.0343	a00-	$(NN)_xDy(N_2)$
1755.5	1697.3	1755.2, 1698.2	1755.3, 1726.9, 1698.3	1.0343	a00−	$(NN)_xDy(N_2)$
1750.6	1692.9	1750.5, 1714.4, 1692.9		1.0341	a00−	$(NN)_xDy(NN)_2$
1744.7	1687.5	1744.7, 1687.5	1744.8, 1716.4, 1687.9	1.0339	a− − −	$(NN)_xDy(N_2)$
1735.0	1677.4	1734.6, 1677.4		1.0343	a0−0	$(NN)_xDy(N_2)$
1462.6	1414.8	1463, 1415		1.0338	a+00	$Dy_x(NN)_y$
1451	1404	1453, 1405	1453, 1430, 1405	1.0335	a+00	$Dy_x(NN)_y$
1374.0	1328.3			1.0344	a+0+	$Dy_x(NN)_y$
1368.1	1322.5			1.0345	b++	$Dy_x(NN)_y$
1206	1166	1207, 1167	1206, 1187, 1167	1.0343	a++−	$Dy_x(NN)_y$
772.8	748.7	772.6, 748.6	772.6, 748.6	1.0322	a+++	$(NN)_xDyN$
678.2	657.3	678.0, 668.0, 657.2	678.0, 667.6, 657.2	1.0318	a− − −	$(NN)_x(DyN)_2$

[a−c] Footnotes same as Table 1.

TABLE 3: Product Absorptions (cm^{-1}) Observed for Laser-Ablated Ho Atoms In Solid Matrices at 10 K

$^{14}N_2$	$^{15}N_2$	$^{14}N_2 + {}^{15}N_2$	$^{14}N_2 + {}^{14,15}N_2 + {}^{15}N_2$	$R(14/15)^b$	anneal.[c]	ident.
			Argon[a]			
2304	2226			1.0350	a+++	
2290.2	2214.2			1.0343	b++	
2124.7	2054.8			1.0340	b++	
2088.9	2019.9			1.0342	a++0	$Ho(NN)_x$
2007.4	1941.3	2007, 1941		1.0340	a+0−	$Ho(NN)_x$
1798.3	1738.6	1798.2, 1738.0	1798.4, 1768.9, 1738.8	1.0343	a+++	$Ho(N_2)$
1763.9	1705.5			1.0342	a+− −(−)	$(NN)_xHo(N_2)$
1752.6	1694.7	1752, 1694		1.0342	a+++	$(NN)_xHo(N_2)$
769.3	745.5			1.0319	b++	$(NN)_xHoN$
701	681			1.029	a− − −	$(HoN)_2$
680.0	659.1			1.0317	b++	$(NN)_x(HoN)_2$
509.4	493.6			1.0320	a− − −	Ho_2N
			Dinitrogen[a]			
2292.4	2216.0	2292.7, 2216.3	2292.8, 2254.8, 2216.4	1.0345	a++0	
2111.6	2041.2	2106.5, 2042.2	2073.5	1.0345	a0− −	$Ho(NN)_x$
1754.7	1696.6	1754.4, 1696.8	1754.5, 1726.0, 1697.0	1.0342	a0+−	$(NN)_xHo(N_2)$
1749.3	1691.2	1749.4, 1691.4	1749.7, 1720.7, 1691.6	1.0343	a0+−	$(NN)_xHo(N_2)$
1596	1543	1596, 1568, 1543		1.0339	a00−(−)	$Ho^+(N_2)_2^-$
1583	1531	1583, 1531		1.0338	a00−(−)	$Ho_x(NN)$
1117.4	1096.2	1117.4, 1096.2	1117.4, 1096.1	1.0193	a0− −	$(NN)_xHo_y(NO)$
769.1	745.3	769.1, 745.3	769.1, 745.3	1.0319	a+++	$(NN)_xHoN$
678.6	657.6	678.4, 667.9, 657.3	678.7, 668.5, 657.8	1.0319	a0− −	$(NN)_x(HoN)_2$
551.9	535.4			1.0308	a0− −	$(NN)_x(HoN)_2$

[a−c] Footnotes same as Table 1.

plexes. The first portion details the identification of the two types of lanthanide nitrides observed for the late lanthanide metals, with a brief description of the analysis of each metal analogue. A third product, Ln_2N, is also tentatively identified for some of the metals, in agreement with previous work.[13,17] The second portion, which deals with molecular nitrogen complexed to a metal center, includes an explanation of each identified complex. Additional unidentified metal dinitrogen

TABLE 4: Product Absorptions (cm^{-1}) Observed for Laser-Ablated Er Atoms In Solid Matrices at 10 K

$^{14}N_2$	$^{15}N_2$	$^{14}N_2 + {}^{15}N_2$	$^{14}N_2 + {}^{14,15}N_2 + {}^{15}N_2$	$R(14/15)^b$	anneal.[c]	ident.
			Argon[a]			
1802	1743	1802, 1743		1.0338	a00−	$Er(N_2)$
1761.6	1703.1	1761.6, 1703.1		1.0343	a000(−)	$(NN)_xEr(N_2)$
			Dinitrogen[a]			
3480.3	3365.7	3479.8, 3366.2	3479.9, 3423.7, 3366.5	1.0340	b+−	$(NN)_xEr(N_2)$
3471.2	3356.6	3470.3, 3357.3	3469.9, 3415.3, 3357.1	1.0341	b+−	$(NN)_xEr(N_2)$
2286.8	2210.8	2287.3, 2210.9	2289.1, 2250.0, 2210.9	1.0344	a++−(−)	
2144.9	2073.8	2144.9, 2074.1		1.0343	a− − −(+)	
2105	2036	2101, 2036	2066	1.0339	a− − −(−)	$Er(NN)_x$
2044	1977	1979		1.0341	a0+−(−)	$Er(NN)_x$
1800.8	1740.7	1800.8, −	1801.0, −	1.0345	a− − −	$Er(N_2)$
1769.7	1710.9	1769.7, 1710.9	1769.7, 1740.6, 1711.0	1.0344	a− − −	$(NN)_xEr(N_2)$
1753.4	1695.3	1753.1, 1695.5	1753.1, 1724.6, 1695.6	1.0343	a0+−	$(NN)_xEr(N_2)$
1748.5	1690.6	1748.4, 1691.1	1748.5, 1720.0, 1691.1	1.0342	a0+−	$(NN)_xEr(N_2)$
1732.2	1674.8	1731.6, 1675.1	1731.6, 1703.6, 1675.1	1.0343	c− −	$(NN)_x Er(N_2)$
1657.5	1603.1	1657.5, 1649.2, 1612.7, 1603.1	1657.6, 1649.2, 1639.9, 1621.3, 1612.8, 1603.2	1.0339	a− − −	N_3
1597	1544	1597, 1568, 1544		1.0343	a−0−(−)	$Er^+(N_2)_2^-$
1582	1530	1582, 1530		1.0340	a−0−(−)	
1544.8	1494.0	1545.0, 1493.9		1.0340	b+−	
1521.1	1471.0	1521.1, 1471.1		1.0341	b+−	
1498.6	1449.3	1498.7, 1449.4	1498.6, 1474.3, 1449.7	1.0340	a0+−(+)	
1117.2	1096.0	1117.4, 1096.0	1117.2, 1095.9	1.0193	a− − −(+)	$(NN)_xEr_y(NO)$
883.3	855.2	883.3, 855.0	883.3, 854.9	1.0329	c0−	
869.8	841.9	870.0, 842.2	869.8, 842.0	1.0331	c− −	
767.8	744.0	767.8, 744.0	767.8, 744.0	1.0320	a++−(−)	$(NN)_xErN$
678.3	657.5	678.3, 668.2, 657.7	678.3, 668.2, 657.7	1.0316	a++−(+)	$(NN)_x(ErN)_2$ B_{3u}

[a−c] Footnotes same as Table 1.

TABLE 5: Product Absorptions (cm^{-1}) Observed for Laser-Ablated Tm Atoms In Solid Matrices at 10 K

$^{14}N_2$	$^{15}N_2$	$^{14}N_2 + {}^{15}N_2$	$^{14}N_2 + {}^{14,15}N_2 + {}^{15}N_2$	$R(14/15)^b$	anneal.[c]	ident.
			Argon[a]			
2283	2207	2284, 2208	2283, 2246, 2209	1.0344	a+++	
2079.5	2010.1	2079, 2012		1.0345	a+0−	$Tm(NN)_x$
1799.5	1740.0	1799.9, 1740.3	1800.1, 1770.7, 1740.3	1.0342	a++0(+)	$Tm(N_2)$
831.8	832.0	831.9	831.5		a− − −	TmO
615.5	615.6	615.3			a− − −	oxide
			Dinitrogen[a]			
3524.3	3407.4			1.0343	c− −	$(NN)_xTm(N_2)$
3482.1	3367.1	3481.5, 3367.5	3481.9, 3425.5, 3367.7	1.0342	a0+0(+)	$(NN)_xTm(N_2)$
3465.7	3351.2			1.0342	c− −	$(NN)_xTm(N_2)$
2286.3	2210.1	2286.4, 2210.0	2286.6, 2248.9, 2210.6	1.0345	a++0	
2097.7	2028.2	2096, 2027	2060	1.0343	a− − −	$Tm(NN)_x$
2084.6	2015.7			1.0342	a− − −	$Tm(NN)_x$
2069.1	2000.4			1.0343	a− − −	$Tm(NN)_x$
2064.0	1996.5			1.0338	a0+0(+)	$(N-N)Tm(N_2)$
2003.2	1937.4	2003.1, 1993.0, 1948.7, 1937.2	2003.3, 1992.7, 1981.9, 1959.4, 1948.7, 1937.2	1.0340	a− − −	N_3^-
1931.7	1868.2	1926, 1870	1927, 1900, 1870	1.0340	a0+0(+)	$(NN)Tm(N_2)$
1921.4	1858.2	1917, 1861	1917, 1891, 1861	1.0340	a0+0(+)	$(NN)Tm(N_2)$
1766.6	1707.9	1765.7, 1708.0	1765.8, 1737.2, 1708.1	1.0344	c− −	$(NN)_xTm(N_2)$
1752.3	1694.2	1751.8, 1694.4	1751.7, 1723.4, 1694.4	1.0343	a0+0(+)	$(NN)_xTm(N_2)$
1740.4	1682.6	1740.1, 1682.3	1740.2, 1711.5, 1682.3	1.0344	c− −	$(NN)_xTm(N_2)$
1657.6	1603.2	1657.5, 1649.1, 1612.8, 1603.0	1657.6, 1649.2, 1639.8, 1621.3, 1612.8, 1603.1	1.0339	a− − −	N_3 radical
1599	1547	1599, 1571, 1547	1599, 1586, 1572, 1560, 1547	1.0336	a00−(−)	$(NN)_xTm^+(N_2)_2^-$
1585	1533	1587, −, 1536		1.0339	a00−(−)	$(NN)_xTm^+(N_2)_2^-$
1459.5	1411.3	1459.6, 1411.3	1460.0, 1436.7, 1411.7	1.0342	a++0(+)	
1365.1	1319.5			1.0346	a+++(−)	
774.1	750.1	774.0, 749.9	774.0, 750.0	1.0320	a+++(−)	$(NN)_xTmN$
684.2	663.3	684.2, 674.1, 663.6	684.1, 674.1, 663.5	1.0315	a++−	$(NN)_x(TmN)_2$ B_{3u}
566.5	549.1	566.4, 556.4, 549.0	566.4, 556.4, 549.1	1.0317	a++−	$(NN)_x(TmN)_2$ B_{2u}
563.4	546.0	563.2, 553.3, 545.9	563.2, 553.4, 546.0	1.0319	a++−	$(NN)_x(TmN)_2$ B_{2u}

[a−c] Footnotes same as Table 1.

complexes are listed in the accompanying tables, but are not discussed in the text. Nitrogen gas samples composed of equimolar concentrations of $^{14}N_2$ and $^{15}N_2$ are termed "mixed" samples; statistical mixtures of $^{14}N_2 + {}^{14}N^{15}N + {}^{15}N_2$ are termed "scrambled" and are obtained by flowing the mixed samples through a microwave discharge, providing randomized samples upon nitrogen recombination.

Nitrides. Two true nitrides are observed in spectra of the laser-ablated late lanthanide metal atoms with N_2, LnN, and $(LnN)_2$. Like their early lanthanide counterparts, frequencies of both molecules in argon redshift as a result of N_2 complexation upon annealing of the matrices.[13] Unlike the early lanthanides, no NLnN dinitride species were observed.

LnN. Of the seven metals encountered in part 2 of this study, only two exhibited the uncomplexed mononitride in solid argon, while all seven formed the mononitride upon deposition into a solid nitrogen film. Nitrogen film frequencies for the mononitrides of all of the lanthanide elements studied are shown in

TABLE 6: Product Absorptions (cm^{-1}) Observed for Laser-Ablated Yb Atoms In Solid Matrices at 10 K

$^{14}N_2$	$^{15}N_2$	$^{14}N_2 + {}^{15}N_2$	$^{14}N_2 + {}^{14,15}N_2 + {}^{15}N_2$	$R(14/15)^b$	anneal.[c]	ident.
			Argon[a]			
2280	2204	2280, 2204		1.035	a00+(+)	$Yb(NN)_x$
2140	2070	2140, 2070		1.034	c0−	$Yb(NN)_x$
1730	1675	1726, 1674		1.033	a00+(+)	$(NN)_xYb(N_2)$
659.8	660.0				a0− −(−)	YbO
627.7	627.7				a00−	YbO_2
604.1	604.2				a00−	oxide
490.7	490.9	490.6			a+++(+)	oxide
			Dinitrogen[a]			
3510.1	3394.2	3509.5, 3394.4, 3386.8		1.0341	a− − −(+)	(NN)Yb(NN)
3468.9	3354.6			1.0341	a++0(+)	$(NN)_xYb(N_2)$
3466.5	3352.1	3465.1, 3352.4	3465.1, 3409.3, 3352.2	1.0341	a++0(+)	$(NN)_xYb(N_2)$ site
2327.5	2249.7	2327.6, 2249.9	2327.7, 2289.0, 2250.0	1.0346	a000(−)	N_2
2279.8	2203.5	2279.8, 2203.5	2280.0, 2242.0, 2203.6	1.0346	a++0(−)	
2176	2105			1.0337	a000(−)	$Yb(NN)_x$
2003.3	1937.5	2003.1, 1992.6, −, 1937.3	2003.1, 1992.6, 1981.3, 1959.3, −, 1937.3	1.0340	a− − −	N_3^-
1988.6	1923.6	1986.9, 1960, −		1.0338	a+00(−)	$Yb(NN)_x$
1976.0	−	1977.6, 1948.5, −	1978, 1964, 1949, 1930, −		a+00(−)	$Yb(NN)_x$ site
1913.5	1850.4	1913.4, 1889.2, 1851.3	1913.6, 1898.7, 1885, 1870.2, 1850.2	1.0341	a+00(−)	$Yb(NN)_x$
1876.9	1815.4			1.0339	a+00(−)	
1862.9	1801.9	1862.4, 1819.5, 1802.0	1826	1.0339	a+00(−)	
1749.1	1691.0	1769.3, 1749.0, 1702.7, 1690.8	1748.9, 1729.0, 1720.1, 1702.7, 1699.8, 1690.8	1.0344	a− − −(+)	(NN)Yb(NN)
1745.2	1687.3			1.0343	a++0(+)	$(NN)_xYb(N_2)$
1744.1	1686.2	1743.4, 1686.4	1743.3, 1715.2, 1686.4	1.0343	a++0(+)	$(NN)_xYb(N_2)$ site
1657.7	1603.4	1657.6, 1649.2, 1612.7, 1603.1	1657.6, 1649.2, 1639.9, 1621.3, 1612.8, 1603.2	1.0339	a+− −	N_3 radical
1611.6	1558.7	1611.7, 1558.7	1611.6, 1585.5, 1558.6	1.0339	a+++(+)	
1582.9	1530.8	1583.1, 1530.6	1583.1, −, 1530.7	1.0340	a+++(−)	
1567.0	1515.4	1567.1, 1515.4	1567.1, 1541.5, 1515.4	1.0341	a+++(−)	
1466.3	1418.0	1466.1, 1417.9	1466.1, 1442.2, 1417.8	1.0341	c++	
1362.8	1317.3			1.0345	a++−(−)	
746.3	721.9	745.8, 721.7	745.9, 721.7	1.0338	a00+	
741.9	719.1	742.0, 719.1	742.0, 719.1	1.0317	a++−(−)	$(NN)_xYbN$
740.5	717.8	740.6, 717.7	740.6, 717.7	1.0316	a++−(−)	$(NN)_xYbN$
739.1	716.5	739.0, 716.2	739.0, 716.2	1.0315	a++−(−)	$(NN)_xYbN$
736.1	713.6	735.8, 713.2	735.8, 713.1	1.0315	a+++	$(NN)_xYbN$
727.1	704.9	727.1, 704.8	727.1, 704.8	1.0315	c− −	$(NN)_xYbN$
648.2	648.1	648.1	648.0		a++0	$(NN)_xYbO$

[a−c] Footnotes same as Table 1.

Figure 1, flanked by the group IIIB and group IVB columns. Methods used to identify the mononitrides have been discussed previously.[13] Typical spectra of N_2 isotopic samples used for identification are shown for holmium in Figure 2. The trend identified for the early lanthanide mononitrides, of isotopic ratios in nitrogen exceeding those in argon, continues for the second half of the lanthanide series and holds, in general, for all metal mononitrides. The effect is similar to substitution of a heavier metal isotope, which causes the ratio to increase, exactly as seen with the calculated harmonic ratios, which are based only on mass and increase continuously from lighter to heavier metals.

The variation in frequency across the lanthanide row differs sharply from the calculated harmonic oscillator mass dependent variation, which decreases smoothly and spans only 7 cm^{-1}, assuming a constant metal−nitride force constant. In contrast, the experimental variation, as measured in nitrogen films (Figure 1), is seemingly erratic and spans 46 cm^{-1}, from PrN at 788.0 cm^{-1} to YbN at 741.9 cm^{-1}. There is no discernible pattern in the frequency distribution across the lanthanide mononitrides. The frequencies remain similar to that of LaN across the row. The discontinuity in frequency from Lu to Hf mirrors the difference, in general, from group IIIB to group IVB metals, roughly categorizing the lanthanide elements with group IIIB.

The predictive power of the argon matrix metal mononitride fundamental frequency is best illustrated for ReN, observed at 1121.7 cm^{-1} (average of 1121.9 and 1121.5 cm^{-1}, ^{185}ReN and ^{187}ReN frequencies, respectively) in the gas phase[8] and at 1117.2 cm^{-1} in solid argon.[11] Allowing that not all metal mononitrides in argon will demonstrate such remarkable consistency with the gas phase, the gas-phase frequencies are estimated by adding 10 cm^{-1} to the argon matrix value and allowing for an error of ±10 cm^{-1}. For those metal systems in which the mononitride is not observed in solid argon, it can be estimated from the frequency observed in solid nitrogen, and then a reasonable prediction can be made for the gas-phase metal mononitride fundamental frequency.

The difference between the argon matrix frequency and the nitrogen film frequency decreases from cerium to dysprosium. This trend is presumed to be upheld for all lanthanide mononitrides, even though only seven have been observed in both argon and nitrogen. The frequency shift upon ligation is mostly the result of a weakening of the metal−nitride bond caused by acceptance of electrons from the dinitrogen ligands into unoccupied orbitals on the metal. The heavier lanthanides are both smaller in volume and have fewer empty orbitals available as electron acceptors, these factors, combined, decrease the number of ligands necessary for saturation. Because there are fewer dinitrogen units complexed to the smaller lanthanides, the effect of ligation on the strength of the metal−nitride bond is decreased, bringing the argon matrix and nitrogen film frequencies closer together. This effect has also been observed for the first row transition metal series.[9,12] The unobserved argon matrix mononitride fundamental predictions are made from the observed nitrogen film frequencies in light of the observed tendency toward convergence of the argon matrix and nitrogen film values across the lanthanide row. Gas-phase values are then predicted by adding 10 cm^{-1} to the estimated argon matrix value, but allowing for an error of ±15 cm^{-1} to compensate for the increased probability of error in the prediction.

TABLE 7: Product Absorptions (cm^{-1}) Observed for Laser-Ablated Lu Atoms In Solid Matrices at 10 K

$^{14}N_2$	$^{15}N_2$	$^{14}N_2 + {}^{15}N_2$	$^{14}N_2 + {}^{14,15}N_2 + {}^{15}N_2$	$R(14/15)^b$	anneal.[c]	ident.
			Argon[a]			
3671.2	3549.9	3671.1, 3549.5	3671.6, 3610.8, 3549.6	1.0342	b++(+)	$Lu(N_2)$
3652.4	3531.4	3652.3, 3531.4	3652.3, 3592.5, 3531.5	1.0343	a− − −(+)	$Lu(N_2)$
2311.0	2234.2			1.0344	b++	
2294.0	2217.4	2293.7, 2217.1	2294, 2255, 2217	1.0345	a+0−(+)	
2271.8	2196.3	2272.3, 2196.7	2273, 2234, 2198	1.0344	b++	
2074.7	2005.8	2074, 2007		1.0344	b++(+)	$Lu(NN)_x$
1845.3	1784.0	1845.2, 1783.8	1845.3, 1814.8, 1783.9	1.0344	a+++(+)	$Lu(N_2)$
1840.2	1779.0	1840.2, 1778.9	1840.1, 1809.7, 1778.9	1.0344	a++−(−)	$Lu(N_2)$
1836.0	1774.9	1836.0, 1774.9	1836.0, 1805.6, 1774.9	1.0344	a− − −(+)	$Lu(N_2)$
1824.3	1763.7	1824.4, 1763.7	1824.4, 1794.3, 1763.7	1.0344	a++0(+)	$Lu(N_2)$
1802	1743			1.0338	b++	$(NN)_xLu(N_2)$
1765.3	1706.4	−, 1706.4		1.0345	a00+(+)	$(NN)_xLu(N_2)$
1758.5	1700.1	1758.5, 1700.0	1758.4, 1729.6, 1700.2	1.0344	a− − −(−)	$(NN)_xLu(N_2)$
1739.0	1681.4	1738.8, 1681.1		1.0343	a00+(+)	$(NN)_xLu(N_2)$
807.0	806.9	806.9	807.0		a− − −	$(NN)_xLuO$
771.4	747.5	771.2, 747.2	771.9, 747.1	1.0320	b++	$(NN)_xLuN$
703.9	682.2	703.9, 682.1	703.9, 693.5, 682.1	1.0318	a−0−	$(LuN)_2$ B_{3u}
701.2	679.6	700.9, 679.3	699.9, 681.1, 679.4	1.0318	b ++	
701.0	679.3	700.9, 679.3	701.0, 690.6, 679.3	1.0319	a−0−	$(LuN)_2$ B_{3u}
674.8	654.0	674.6, 653.7	675.1, 664.8, 654.0	1.0318	b++	$(NN)_x(LuN)_2$ B_{3u}
601.0	582.4	600.9, 582.3	600.7, 585.6, 582.7	1.0319	b++	
589.9	571.7	590.1, 571.8	589.8, 579.3, 571.5	1.0318	a00−	$(LuN)_2$ B_{2u}
587.7	569.6	587.7, 569.5	587.7, 577.1, 569.6	1.0318	a00−	$(LuN)_2$ B_{2u}
583.4	565.3	583.4, 565.4	584, 573, 566	1.0320	a− − −	$(NN)_x(LuN)_2$ B_{2u}
568.8	551.3	568.7, 551.0	568.6, 558.5, 551.0	1.0317	b++	$(NN)_x(LuN)_2$ B_{2u}
563.7	547.8	563.4, 547.5	561.6, 553.7, 547.9	1.0290	b++	$(NN)_x(LuN)_2$ B_{2u}
522.0	505.6	522.2, 505.2	522, 506	1.0324	a− − −	Lu_2N
513.4	497.3	512.9, 497.4		1.0324	b++	$(NN)_xLu_2N$
			Dinitrogen[a]			
3678.5	3556.8			1.0342	a++−(−)	$Lu(N_2)$
3668.7	3547.5			1.0342	a+++(−)	$Lu(N_2)$
2327.2	2249.5	2327.7, 2250.0	2327.7, 2289.2, 2250.0	1.0345	a−00(−)	N_2
2272.8	2197.2	2273.1, 2197.4	2273.1, 2235.6, 2197.5	1.0344	a+++(−)	
2132.1	2061.5	2132.1, 2061.8	2131.9, −, 2061.9	1.0342	a++0	
2094	2025	2089, 2023	2075	1.0341	a−0−(−)	$Lu(NN)_x$
2078	2010			1.0338	a−0−(−)	$Lu(NN)_x$
2003.1	1937.4	2003.1, 1992.8, 1949.7, 1937.6	2003.3, 1992.7, 1981.9, 1959.4, 1948.7, 1937.6	1.0339	a− − −	N_3^-
1992.5	1926.5			1.0343	a− − −(−)	$Lu(NN)_x$
1898.3	1835.7			1.0341	a− − −(−)	
1896.1	1833.5			1.0341	a− − −(−)	
1852.0	1790.4	1852.1, 1790.4	1852.0, 1821.4, 1790.3	1.0344	a− − −(−)	$Lu(N_2)$
1848.9	1787.4	1849.0, 1787.4	1849.0, 1818.3, 1787.4	1.0344	a++−(−)	$Lu(N_2)$
1846.0	1784.6	1846.1, 1784.7	1846.1, 1815.6, 1784.7	1.0344	a− − −	$Lu(N_2)$
1844.2	1782.8	1844.2, 1782.8	1844.2, 1813.8, 1782.8	1.0344	a+++(−)	$Lu(N_2)$
1839.5	1778.3	1839.6, 1778.4	1839.5, 1809.2, 1778.3	1.0344	a+− −(−)	$Lu(N_2)$
1800.2	1740.6			1.0342	a++0(−)	$(NN)_xLu(N_2)$
1797.3	1737.6			1.0344	a++0(−)	$(NN)_xLu(N_2)$
1787.3	1727.9	−, 1727.9	−, 1755.9, 1727.7	1.0344	a− − −(−)	$(NN)_xLu(N_2)$
1765.3	1706.5	1765.3, 1706.6	1765.3, 1736.3, 1706.6	1.0345	a− − −(−)	$(NN)_xLu(N_2)$
1753.4	1695.1	1753.0, 1695.6	1753.0, 1724.6, 1695.6	1.0344	a++−	$(NN)_xLu(N_2)$
1748.0	1689.9	1747.6, 1690.3	1747.6, 1719.3, 1690.3	1.0344	a+++	$(NN)_xLu(N_2)$
1744.3	1686.4	1744.0, 1686.8	1744.0, 1717.4, 1686.9	1.0343	a0++	$(NN)_xLu(N_2)$
1737.7	1680.0	1737.7, 1680.0	1737.6, 1709.1, 1680.0	1.0343	a+00(+)	$(NN)_xLu(N_2)$
1735.5	1677.8	1735.6, 1677.9	1735.5, 1707.0, 1677.9	1.0344	a0+−(+)	$(NN)_xLu(N_2)$
1657.4	1603.1	1657.5, 1649.2, 1612.8, 1603.1	1657.6, 1649.1, 1639.8, 1621.2, 1612.7, 1603.1	1.0339	a− − −(−)	N_3 radical
1600	1547			1.0343	a00−(−)	$(NN)_xLu^+(N_2)_2^-$
1589	1537			1.0338	a00−(−)	$(NN)_xLu^+(N_2)_2^-$
1175.0	1136.6	1174.7, 1136.4	1174.7, 1155.7, 1136.4	1.0338	a+++	
770.8	746.8	770.9, 746.9	770.9, 746.9	1.0321	a+++(−)	$(NN)_xLuN$
701.4	679.6	701.5, 679.8	701.3, 679.7	1.0321	b++	
675.2	654.2	675.1, 665.2, 654.3	675.1, 665.1, 654.4	1.0321	a+++(+)	$(NN)_x(LuN)_2$ B_{3u}
604.9	585.7		604.8, 585.9	1.0328	a000(+)	
581.4	563.5			1.0318	a+++(+)	
569.6	551.8	569.6, 559.3, 551.9	569.6, 559.3, 551.9	1.0323	a++0(+)	$(NN)_x(LuN)_2$ B_{2u}
513.3	497.2			1.0324	a+++(+)	$(NN)_xLu_2N$

[a−c] Footnotes same as Table 1.

TbN. Terbium mononitride is observed both in argon and in nitrogen matrices. In argon, the band at 805.3 (780.4) cm^{-1} is assigned to TbN (^{15}N counterpart in parentheses). This band shows no central component in either the mixed or scrambled isotopic samples and exhibits an isotopic ratio of 1.0319, compared to the calculated harmonic oscillator ratio of 1.0320. In nitrogen, the fully ligated counterpart appears at 764.6 (740.9) cm^{-1}, yielding an isotopic ratio of 1.0320, and grows dramatically with annealing of the nitrogen matrix. As expected, anharmonicity causes the isotopic ratio to decrease slightly from the calculated harmonic value. In solid nitrogen, however, damping of the metal motion by N_2 ligation effectively cancels

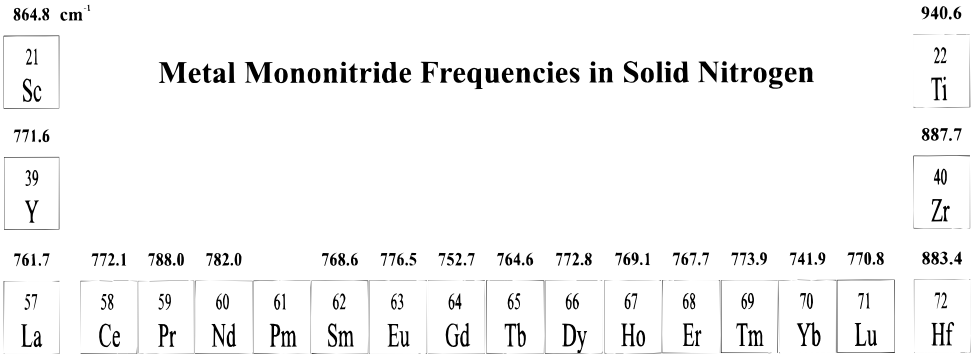

Figure 1. Infrared absorption frequencies (cm^{-1}) of the group IIIB, group IVB, and lanthanide metal mononitrides observed in solid $^{14}N_2$ matrices.

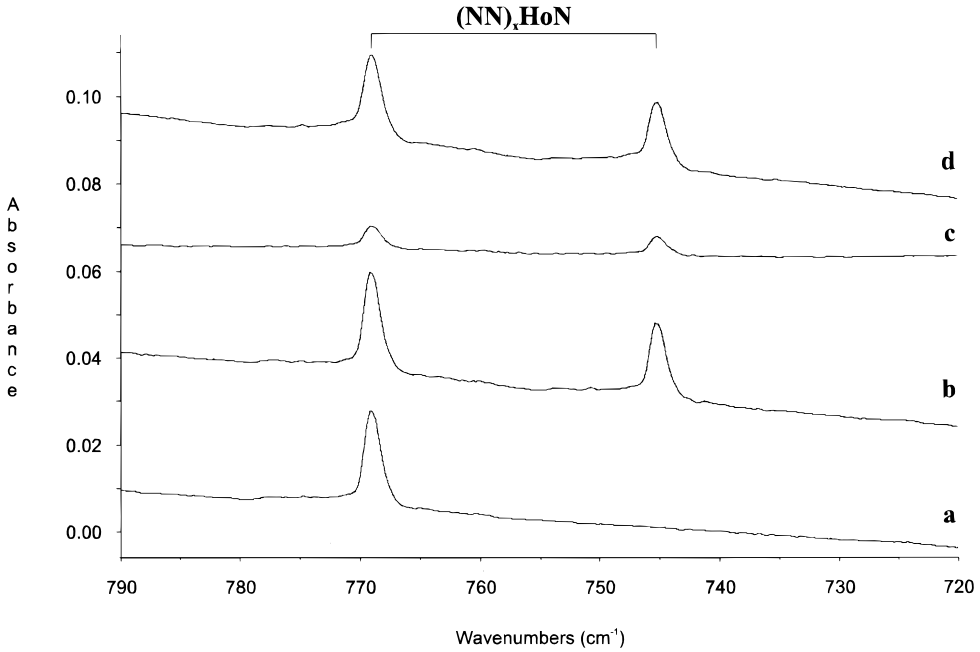

Figure 2. Infrared spectra in the 790−720 cm^{-1} region for laser-ablated holmium atoms deposited into a: (a) $^{14}N_2$ film, (b) $^{15}N_2$ film on top of the $^{14}N_2$ film, (c) mixed N_2 film, (d) scrambled N_2 film.

the anharmonic contribution and renders an isotopic ratio in agreement with the harmonic oscillator. TbN is predicted to absorb in the gas phase at 815 ± 10 cm^{-1}.

DyN. Like TbN, DyN appears in both solid argon and nitrogen. The argon matrix bands are only weakly observed at 810.5 (785.5) cm^{-1}, while the nitrogen peaks are strong and sharp. The isotopic pattern is plainly observed in the nitrogen film spectra which show the $Dy^{14}N$ ($Dy^{15}N$) absorption at 772.8 (748.7) cm^{-1}. The isotopic ratio of 1.0318 in argon and 1.0322 in nitrogen is appropriate for the harmonic-oscillator ratio, with minor adjustment for anharmonicity. In the gas phase, DyN is predicted at 820 ± 10 cm^{-1}.

HoN. HoN appears prominently at 769.1 (745.2) cm^{-1} upon deposition in nitrogen films (Figure 2). Although the mononitride is not observed upon deposition in argon matrices, the complexed molecule is observed at 769.3 cm^{-1} after annealing to 45 K. It can therefore be confirmed that the mononitride does indeed exist in argon matrices, but its uncomplexed value cannot be determined. In view of the $(NN)_xHoN$ observations, uncomplexed HoN is expected to absorb at about 805 cm^{-1} in solid argon and therefore at 815 ± 15 cm^{-1} in the gas phase.

ErN. The sharp nitrogen matrix peak observed at 767.7 (743.9) cm^{-1} is assigned to the vibration of the ErN diatomic. The molecule is not observed in argon matrices, but is expected to absorb at about 800 cm^{-1} on the basis of extrapolation from the mononitrides that were observed under both conditions. This value is obtained by assuming that the observed convergence of the argon and nitrogen film values continues throughout the lanthanides, approximating ErN in argon to be about 30 cm^{-1} higher than ErN in nitrogen. ErN is predicted in the gas phase at 810 ± 15 cm^{-1}.

TmN. $Tm^{14}N$ ($Tm^{15}N$) absorbs in solid nitrogen at 774.2 (750.1) cm^{-1}. The absorption due to this molecule increases with each of three successive annealings and decreases by about one-third with broadband UV photolysis. Its nitrogen isotopic 14/15 ratio of 1.0321 is in good agreement with the harmonic ratio of 1.0322. The isotopic doublet for this molecule in the scrambled N_2 film experiment secures the assignment. TmN does not absorb intensely enough in argon matrix experiments to be observed, but extrapolation from the nitrogen film value allows approximation of the argon matrix frequency at 805 cm^{-1}. TmN is expected to absorb in the gas phase at 815 ± 15 cm^{-1}.

YbN. An absorption observed at 742.1 (719.1) cm^{-1} in spectra of Yb deposited in solid $^{14}N_2$ ($^{15}N_2$) is attributed to $Yb^{14}N$ ($Yb^{15}N$). With successive annealing cycles, this broad absorption increases and splits into four well-defined sites appearing at 741.9 (719.1), 740.5 (717.8), 739.1 (716.5), and 736.1 (713.6) cm^{-1}. Photolysis decreases the peaks by half. All of the observed sites exhibit isotopic ratios consistent with the harmonic ratio

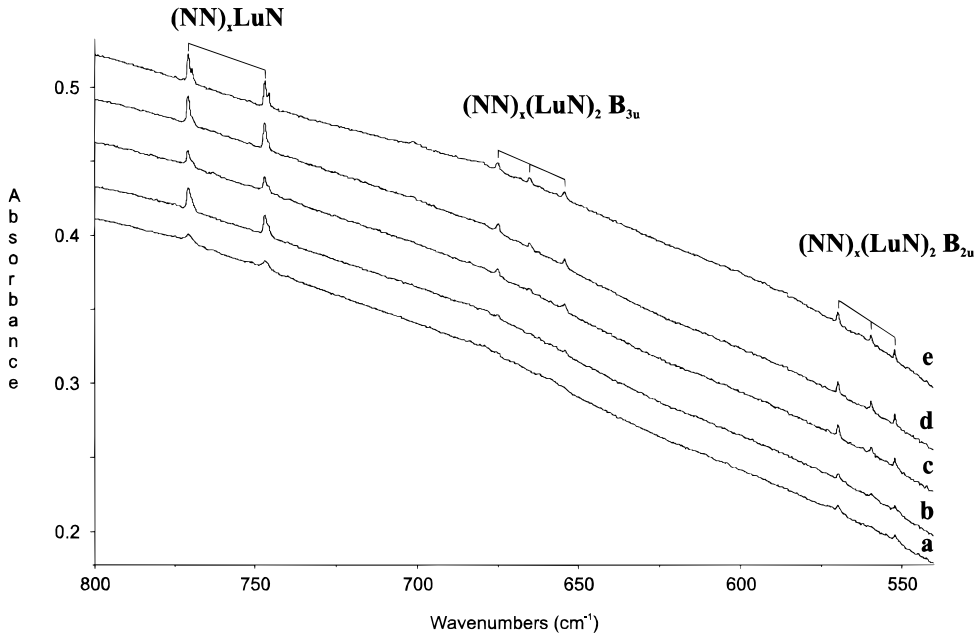

Figure 3. Infrared spectra in the 800−540 cm^{-1} region for laser-ablated lutetium atoms deposited into a mixed N_2 film: (a) after 20 min deposition, (b) after annealing to 25 K, (c) after 15 min broadband UV photolysis, (d) after annealing to 30 K, (e) after annealing to 35 K.

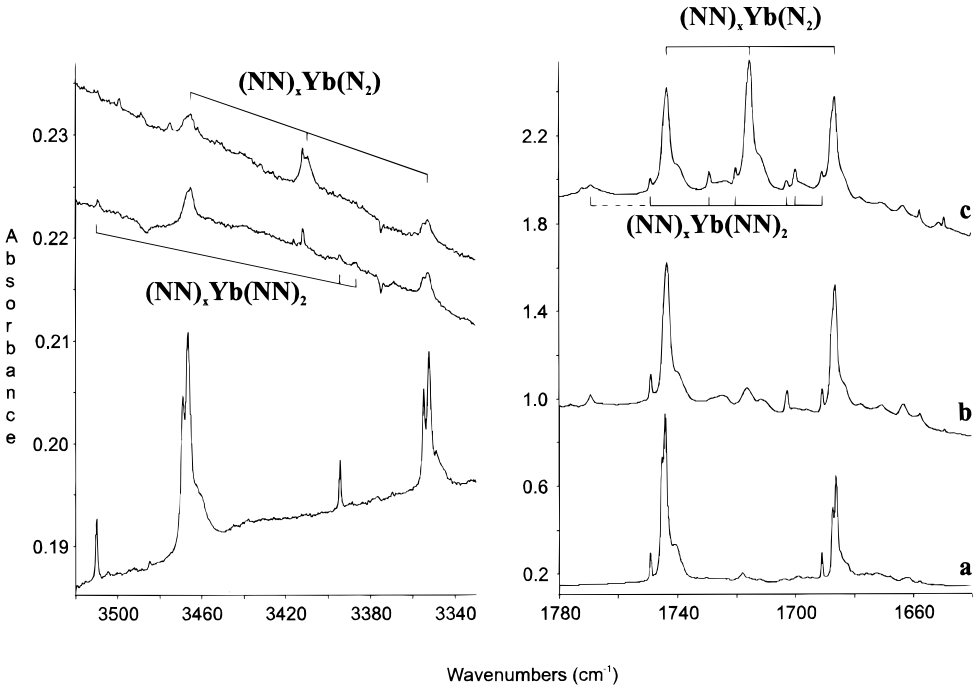

Figure 4. Infrared spectra in the 3520−3330 and 1780−1640 cm^{-1} regions for laser-ablated ytterbium atoms deposited into a: (a) $^{14}N_2$ film + $^{15}N_2$ film after 20 min broadband UV photolysis, (b) mixed N_2 film after 20 min photolysis, (c) scrambled N_2 film after 15 min photolysis. Absorbance-scale fits trace a; traces b and c have been enhanced relative to a.

of 1.0322. The isotopic doublet without intermediate components found in the scrambled nitrogen film confirms the assignment. The argon absorption frequency, although not observed, is anticipated to be near 770 cm^{-1}, and the gas-phase value is predicted at 780 ± 15 cm^{-1}.

LuN. A prominent absorption in solid nitrogen at 770.8 (746.8) cm^{-1}, that increases with annealing and decreases with photolysis, is assigned to $Lu^{14}N$ ($Lu^{15}N$). After annealing to 35K, a secondary site is observable at 769.9 (745.9) cm^{-1}. The uncomplexed LuN frequency in solid argon is too weak to observe in these experiments; however, after annealing, the complexed $(NN)_xLuN$ absorption that was observed in the nitrogen film experiments (Figure 3) appears and increases with successive annealings. The argon matrix counterpart is expected to absorb near 800 cm^{-1}, and the gas-phase value is predicted at 810 ± 15 cm^{-1}.

$(LnN)_2$. The identifying characteristics of the $(LnN)_2$ molecule, also known as $Ln(\mu\text{-}N)_2Ln$, are a nitrogen isotopic ratio near that of the corresponding mononitride and an isotopic triplet of peaks with scrambled N_2 samples, indicative of two N atoms present in the vibration, and these have been discussed in the preceding paper at greater length.[13] Of the 13 lanthanide nitride systems studied, only Eu and Yb have not been observed to form an $(LnN)_2$ molecule. Atomic Eu contains a half-filled f shell and no d electron; atomic Yb has a complete f shell and

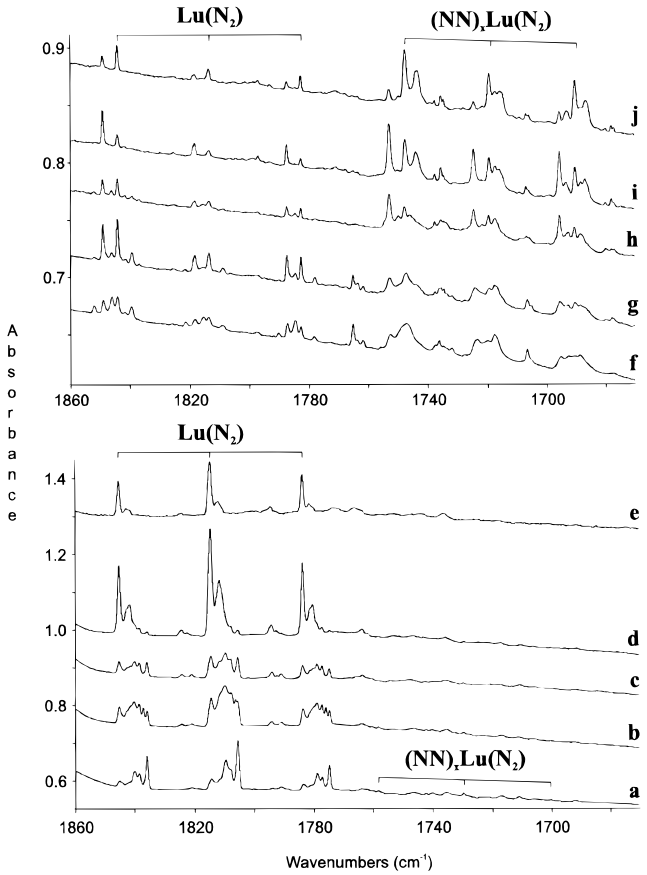

Figure 5. Infrared spectra in the 1860−1670 cm^{-1} region for laser-ablated lutetium atoms co-deposited with scrambled N_2. Bottom (5% in Ar): (a) after 1.5 h deposition, (b) after annealing to 25 K, (c) after 15 min broadband UV photolysis, (d) after annealing to 35 K, (e) after annealing to 45 K. Top (100% mixed + scrambled N_2 film): (f) after 20 min deposition, (g) after annealing to 25 K (h) after 15 min broadband UV photolysis, (i) after annealing to 30 K, (j) after annealing to 35 K.

no d electron. Both B_{2u} and B_{3u} modes are identified for several of the rhombic rings, but for some, only the B_{3u} mode is observed.

Relative to their early lanthanide counterparts, $(LnN)_2$ molecules containing the later lanthanides absorb more strongly in N_2 films, with $(ErN)_2$ and $(TmN)_2$ observed only in nitrogen matrices. Previously, the rhombic rings absorbed more strongly in argon matrices and only weakly in nitrogen. This trend supports the claim that LnN molecules complex fewer dinitrogen ligands as the metal center decreases in size across the lanthanide series. Formation mechanisms for $(LnN)_2$ discussed in the previous work show that in solid nitrogen the $(LnN)_2$ molecule forms primarily by dimerization of the LnN precursor, but postulate that this process is inhibited by the presence of dinitrogen ligands on the metal center. With fewer ligands, the dimerization process is more facile, yielding greater quantities of the dimer in nitrogen films relative to the early lanthanide counterparts. It is also noted, and clearly demonstrated for $(LuN)_2$ in Figure 3, that for the later lanthanides in solid nitrogen, the rhombic ring forms both through dimerization, mentioned for the early lanthanides, and through addition of atomic Ln to an $Ln(N_2)$ complex. In the Lu + N_2 system, the extreme case is demonstrated, whereby formation of the ring upon deposition occurs through the side-bound dinitrogen complex, but formation upon annealing of nitrogen films containing atomic lutetium occurs by dimerization of LuN, evidenced by the appearance of a central component, converting the original doublet of peaks found for the B_{2u} mode of $(LuN)_2$, upon deposition with a mixed $^{14}N_2$ + $^{15}N_2$ nitrogen isotopic sample, to a triplet of peaks of nearly equal intensity following the 35K annealing. The weaker B_{3u} mode mirrors this pattern.

$(TbN)_2$. As usual, the rhombic dimer appears in both the nitrogen film and argon matrix experiments. Both B_{2u} and B_{3u} modes are observed at 550.9 (534.4) and 669.4 (648.9) cm^{-1}, respectively, in nitrogen films and at 569.3 (552.4) and 696.9 (675.8) cm^{-1}, respectively, in argon matrices. In agreement with the early lanthanides, $(TbN)_2$ absorbs more strongly in argon matrices than in nitrogen films. In mixed nitrogen films, although a central component is present, it is less intense upon deposition than the pure isotopic peaks flanking it on either side. After annealings, the central peak increases relative to its pure isotopic counterparts, exceeding them after annealing to 33 K. Scrambled N_2 film experiments maintain a 1:2:1 isotopic triplet for both observed modes throughout the experiment.

Two possible reaction mechanisms detailed previously are pertinent to this system as well. Clearly, in argon the mixed isotopic doublet indicates that only one dinitrogen unit is involved in the reaction, making it likely that the formation mechanism involves a side-bound N_2 complex. In nitrogen, however, it appears that both mechanisms, the one proceeding through the N_2 complex and the direct dimerization of TbN, are active upon deposition, which explains the weaker intensity in the central component of the isotopic triplets relative to their adjacent isotopic counterparts. Annealing favors the dimerization route of formation, causing the central components to intensify relative to the outside peaks of the isotopic triplets.

$(DyN)_2$. The B_{3u} mode of the rhombic dimer of DyN is observed at 678.2 (657.3) cm^{-1} in nitrogen film experiments and at 701.9 (681.8) cm^{-1} in argon matrices. The B_{2u} mode is not observed in either case. The uncomplexed absorption in argon is broad and indistinct, but sharpens considerably upon complexation, while red-shifting nearly to the nitrogen film value. The same interplay between the central component and the adjacent pure isotopic absorptions in the mixed isotopic triplet is observed for $(DyN)_2$ as was observed for $(TbN)_2$, indicating identical mechanisms of formation.

$(HoN)_2$. This molecule is more prominent in nitrogen films than in argon matrices. It absorbs in nitrogen at 678.6 (657.6) cm^{-1} with a central isotopic component found in mixed and scrambled nitrogen films at 668.5 cm^{-1}. Like its predecessors, the mixed nitrogen film exhibits a 1:1:1 isotopic splitting upon deposition, while the scrambled nitrogen film shows the characteristic 1:2:1 isotopic splitting, indicating that two different mechanisms of reaction are active on deposition into solid nitrogen, but that dimerization is the dominant formation method upon annealing. The increased facility of the dimerization mechanism moving across the row may be partially due to the decrease in N_2 ligands surrounding the LnN precursor, as explained in the LnN section.

A broad absorption found upon deposition of Ho into a 4% $^{14}N_2$ ($^{15}N_2$) mixture in argon at 700.8 (681.3) cm^{-1} is attributed to the B_{3u} mode of uncomplexed $(HoN)_2$. This absorption is too weak to observe in mixed and scrambled nitrogen samples in argon. In the pure $^{14}N_2$ ($^{15}N_2$) isotopic sample, annealing red-shifts the observed peak to 680.0 (659.1) cm^{-1}, close enough to the values found in the nitrogen film experiments to positively identify the species.

$(ErN)_2$. No erbium nitride products were observed in argon matrices. In nitrogen films, the B_{3u} mode of $(Er^{14}N)_2$ ($(Er^{15}N)_2$) absorbs at 678.3 (657.6) cm^{-1}. Mixed and scrambled nitrogen films provide a central isotopic component at 668.3 cm^{-1} which

increases relative to its pure isotopic neighbors with annealing of the mixed nitrogen film, as detailed for the previous metals.

$(TmN)_2$. Like erbium, thulium nitride products were also unobserved in argon matrices. Both the B_{3u} and B_{2u} modes of $(Tm^{14}N)_2$ ($(Tm^{15}N)_2$) were observed in nitrogen films at 684.1 (663.3) and 566.5 (549.1) cm^{-1}, respectively. These peaks increase with photolysis while the corresponding mononitride peaks diminish, indicating that UV photons assist the dimerization.

$(LuN)_2$. The B_{3u} mode of $(Lu^{14}N)_2$ ($(Lu^{15}N)_2$) absorbs strongly in argon at 705.5 (683.8) cm^{-1}; the B_{2u} mode absorbs at 589.9 (571.7) cm^{-1}. In nitrogen films, both modes are also observed at 675.3 (654.3) and 569.6 (551.8) cm^{-1}, respectively. Of all the $(LnN)_2$ molecules under consideration, $(LuN)_2$ provides the most clear example of production by two different mechanisms in the nitrogen film experiments, as was mentioned for the Ho analogue. The mixed nitrogen film provides a clear isotopic doublet upon deposition, but with annealing the central isotopic component appears, achieving the same intensity as the pure isotopic peaks following 35 K annealing (Figure 3). As in all the other cases, in argon the rhombic ring forms only by the side-complexed intermediate, not by dimerization of LuN, which is attested by the mixed nitrogen isotopic doublet.

Ln_2N. Absorptions found approximately 200 cm^{-1} lower than the higher of the two rhombic-ring modes are tentatively assigned to the Ln_2N ring molecule. This three-membered ring is assigned in argon matrices for Tb, Dy, Ho, and Lu and in nitrogen films for Tb and Lu. In argon matrices only, the mixed and scrambled nitrogen isotopic components of this peak were observed for Tb, Dy, and Lu; in mixed and scrambled nitrogen films, the peaks were too weak to be observed. From the argon data, it is observed that in mixed and scrambled experiments no central component is present in the isotopic doublet. This makes it clear that only one nitrogen atom is involved in the stretch and allows assignment to the Ln_2N molecule, analogous to the previously assigned early lanthanide spectra and the iron + nitrogen system.[17] In all cases, the isotopic ratio observed for this peak is greater than the ratio of the diatomic mononitride, which is evidence that the angle at the nitrogen apex is smaller than 90°. This continues the trend begun in the previous paper; Pr_2N and Nd_2N have apex angles greater than 90°, but Eu_2N, Gd_2N, Tb_2N, Dy_2N, Ho_2N, and Lu_2N have nitrogen apex angles less than 90°.[13] Except for Eu, this is consistent with the decrease in the M−M bond length observed across the lanthanide row. Since bonding is likely to be similar for all the lanthanides, it is reasonable that a decrease in the metal−metal bond coincides with a decrease in the apex angle of the triangle.

Dinitrogen Complexes. There are two basic orientations of dinitrogen with respect to a complexed Ln metal center: end-bound, (η^1−N_2) or (NN), and side bound, (η^2−N_2) or (N_2). Commonly identified complexes include $Ln(N_2)$, $Ln(NN)_2$, and $Ln(NN)_x$, the coordinately saturated metal center. The $Ln(NN)_2$ species exhibits absorptions in the mid 1700 cm^{-1} region, and $Ln(N_2)$ shows absorption sites ranging from the mid 1700-cm^{-1} to the mid 1800-cm^{-1} region. The fully coordinated metal center, presumably with end-bound dinitrogens, absorbs near 2100 cm^{-1}. Previous thermal lanthanide metal atom reactions[25] provide the saturated metal complex at 2135 cm^{-1} for Sm deposited into pure dinitrogen but no true nitride absorptions below 1000 cm^{-1}. Similar results have been obtained for other Ln metals.[26] Clearly the laser-ablation process is necessary to create atomic N for reaction to form metal nitrides. Other unidentified peaks reported in Tables 1−7 that exhibit N−N stretching ratios and range from 1800 to as low as 1200 cm^{-1} may be attributed to various N_2 complexes of one or both of the above types, but with an indeterminate number of ligands and metal centers.

$Ln(N_2)$. The most prevalent dinitrogen complex with the last seven lanthanide metals is the side-bound $Ln(N_2)$ complex, which occurs for all seven metals both in argon and nitrogen matrices. It is identified by the isotopic triplet of peaks found in scrambled N_2 samples and the isotopic nitrogen ratio, which is appropriate for an N−N stretch (Figure 4). All except Ho-(N_2) exhibit the first overtone of the observed nitrogen fundamental under nitrogen film conditions; $Lu(N_2)$ additionally provides this overtone under argon matrix conditions.

As can be determined from Tables 1−7, the several sites usually present for this species can be grouped into two primary sets of peaks, differing from 50 to 100 cm^{-1} in value. The observed overtone bands can be traced to one or the other of the primary sets, but not both; this varies with the metal. In argon matrices, the higher of the two primary sets is most prominent, while in nitrogen films, the lower dominates and the higher set is often not present, which provides reason to conclude that the higher set of peaks is due to the uncomplexed $Ln(N_2)$ species, while the lower set can be associated with the dinitrogen complexed $(NN)_xLn(N_2)$ species (Figure 5). Experiments with the early lanthanides yielded the lower, complexed peak, in quantity, but did not generally provide the uncomplexed species. This is consistent with all that has been previously stated with regard to the more facile dinitrogen complexation of the early lanthanide metals as compared with the late lanthanide metals. The overtones observed clearly track with the fundamental through annealing and photolysis cycles and exhibit identical nitrogen isotopic splitting.

$Ln(NN)_2$. $Ln(NN)_2$ is the other identifiable complex that is commonly found in lanthanide nitride systems. For the latter half of the lanthanides, this complex has been identified in dinitrogen with Tb, Dy, and Yb, but in argon only with Tb. As explained in the previous paper, the nitrogen isotopic splitting of this complex shows that there are exactly two nitrogen molecules involved in the vibration and the ratio is appropriate for an N−N stretch (Figure 4), and the overtones of the fundamentals are observed about 10 cm^{-1} higher than twice the fundamentals.[13] Previously, this unusual anharmonic contribution has been attributed to the high symmetry of the complex, which is proposed to be linear. As a result of the lack of intensity of these bands, in general, and the further reduction in intensity with mixed and scrambled isotopic nitrogen samples, the overtones were not found in mixed or scrambled experiments prior to the analysis of the Yb + N_2 spectra, for which the mixed counterparts were identified, but the scrambled were still too weak to observe (Figure 4). In the mixed samples, the overtone of the (^{14}N−^{14}N)Yb(^{15}N−^{15}N) shows negative anharmonicity of about 20 cm^{-1}, common to the overtones of $Ln(N_2)$, rather than the positive anharmonicity seen with its pure nitrogen isotopic counterparts. This evidence supports the previous attribution of the unusual positive anharmonicity to the symmetry of the complex, which is broken in the mixed isotope analogue.

$Ln(NN)_x$. Peaks attributed to the fully complexed metal center were observed in both argon and nitrogen matrices for all systems except Er + N_2, for which the complex was observed only in nitrogen films. In Tables 1−7, the highest peak, labeled $Ln(NN)_x$, is attributed to the fully complexed metal center, where the value of x is unknown. Because this absorption is so broad, the mixed isotopic peaks vary several wavenumbers from the pure isotopic peaks, and the scrambled isotopic spectrum

coalesces into a single broad peak between the two pure nitrogen isotopic absorptions.

$Ln^+(N_2)_2^-$. Found only in nitrogen films with laser-ablated Tb, Ho, Er, Tm, and Lu atoms, this broad peak exhibits an isotopic triplet in mixed $^{14}N_2 + {}^{15}N_2$ samples and an isotopic quintet in scrambled samples. It is therefore due to a species containing two dinitrogen units and is tentatively assigned to the $Ln^+(N_2)_2^-$ complex. Like the previous analogues assigned to the early lanthanides, this peak decreases upon photolysis, consistent with an anionic species.

Conclusions

The mononitrides and mononitride dimers of the last seven lanthanide metals have been reported here for the first time. As with the early lanthanide metals, both were observed to shift to lower frequencies upon complexation of dinitrogen.[13] In several cases, although the mononitride was not observed in isolation in argon matrix experiments, annealing revealed the dinitrogen complexed mononitride, universally observed in nitrogen films. An observed tendency toward convergence of the complexed and uncomplexed mononitrides with progression across the lanthanide series provides the conclusion that saturation of the mononitride by dinitrogen ligands is achieved at lower coordination numbers with the heavier, and radially smaller, metals.

In addition, the two dinitrogen complexes, $Ln(N_2)$ and $Ln(NN)_2$ have been identified. A connection has been established between the propensity of $Ln(N_2)$ to complex additional dinitrogen units and the later activity of the $Ln(N_2)$ species. Addition of dinitrogen ligands to the $Ln(N_2)$ complex deactivates it toward further reaction. It has been found that the early lanthanides and early lanthanide nitrides more readily complex dinitrogen than do their late lanthanide counterparts and that the late lanthanides and their nitrides achieve dinitrogen saturation at lower coordination numbers than the early lanthanides, which properties, together, allow the late lanthanide $Ln(N_2)$ species to participate in the formation of $(LnN)_2$ even in a nitrogen film environment. This is, in all cases, the sole method of formation in an argon matrix, but it was not observed to occur in nitrogen films for the early lanthanide analogues. Only Eu and Yb have not been observed to form the $(LnN)_2$ ring under either circumstance; these metals contain a half-filled f shell with zero d electrons and a full f shell with zero d electrons, respectively. The early lanthanide analogues of the side-bound dinitrogen complex are in general more reactive than their late lanthanide counterparts. For early lanthanides, both the $(NN)_xLn(N_2)$ and the $(LnN)_2$ species were formed on deposition, but not the isolated $Ln(N_2)$ complex; in contrast, the late lanthanide metals allowed isolation of the $Ln(N_2)$ species.

Acknowledgment. We gratefully acknowledge financial support from National Science Foundation Grant CHE 97-00116.

References and Notes

(1) Gingerich, K. A. *J. Chem. Phys.* **1971**, *54*, 3720.
(2) Azzaro, M.; Breton, S.; Decouzon, M.; Geribaldi, S. *Int. J. Mass Spectrom. Ion Processes* **1993**, *128*, 1.
(3) Kilbourn, B. T. *J. Less-Common Met.* **1985**, *111*, 1.
(4) Evans, W. J.; Olofson, J. M.; Ziller, J. W. *Inorg. Chem.* **1989**, *28*, 4308.
(5) Mehrotra, R. C.; Singh, A.; Tripath, U. M. *Chem. Rev.* **1991**, *91*, 1287.
(6) Douglas, A. E.; Veillette, P. J. *J. Chem Phys.* **1980**, *72*, 5378.
(7) Berezin, A. B.; Dmitvuk, S. A.; Kataev, D. I. *Opt. Spektrosk.* **1990**, *68*, 310.
(8) Ram, R. S.; Bernath, P. F.; Balfour, W. J.; Cao, J.; Qian, C. X. W.; Rixon, S. J. *J. Mol. Spectrosc.* **1994**, *168*, 350.
(9) Kushto, G. P.; Souter, P. F.; Chertihin, G. V.; Andrews, L. *J. Chem. Phys.*, in press.
(10) Andrews, L.; Souter, P. S.; Bare, W. D.; Liang, B., to be submitted.
(11) Zhou, M.; Andrews, L. *J. Phys. Chem. A* **1998**, *102*, 9061.
(12) Andrews, L. *J. Electron Spectrosc. Relat. Phenom.* **1998**, *97*, 63.
(13) Willson, S. P.; Andrews, L. *J. Phys. Chem. A* **1998**, *102*, 10238.
(14) Evans, W. J.; Ulibarri, T. A.; Ziller, J. W. *J. Am. Chem. Soc.* **1988**, *110*, 6877.
(15) Desmangles, N.; Jenkins, H.; Ruppa, K. B.; Gambarotta, S. *Inorg. Chim. Acta* **1996**, *250*, 1.
(16) Lee, D. W.; Kaska, W. C.; Jensen, C. M. *Organometallics* **1998**, *17*, 1.
(17) Chertihin, G. V.; Andrews, L.; Neurock, M. *J. Phys. Chem.* **1996**, *100*, 14609.
(18) Andrews, L.; Bare, W. D.; Chertihin, G. V. *J. Phys. Chem. A* **1997**, *101*, 8417.
(19) Burkholder, T. R.; Andrews, L. *J. Chem. Phys.* **1991**, *95*, 8697.
(20) Hassanzadeh, P.; Andrews, L. *J. Phys. Chem.* **1992**, *96*, 9177.
(21) Tian, R.; Facelli, J. C.; Michl, J. *J. Phys. Chem.* **1988**, *92*, 4073.
(22) DeKock, R. L.; Weltner, W., Jr. *J. Phys. Chem.* **1971**, *75*, 514.
(23) Gabelnick, S. D.; Reedy, G. T.; Chasanov, M. G. *J. Chem. Phys.* **1974**, *60*, 1167.
(24) Willson, S. P.; Andrews, L. *J. Phys. Chem. A*, in press.
(25) Klotzbücher, W. E.; Petrukhina, M. A.; Sergeev, G. B. *Mendeleev. Commun.* **1994**, *5*.
(26) Klotzbücher, W. E., unpublished results.